

Pairing with dominant triplet component and possible weak topological superconductivity in BiS₂-based superconductors

Yang Yang,¹ Wan-Sheng Wang,¹ Yuan-Yuan Xiang,¹ Zheng-Zao Li,¹ and Qiang-Hua Wang¹

¹*National Laboratory of Solid State Microstructures, Nanjing University, Nanjing, 210093, China*

We show that the newly discovered BiS₂-based superconductors may have a dominant triplet pairing component, in addition to a subdominant singlet component arising from the spin-orbital coupling. The pairing respects time-reversal symmetry. The dominant triplet gap causes gap sign changes between the spin-split Fermi pockets. Within a pocket, the gap function respects $d_{x^2-y^2}^*$ -wave symmetry, where the star indicates joint spin-lattice rotations. Below the Lifshitz filling level the gap is nodeless and the superconducting state is weak topological. Above the Lifshitz points the gap becomes nodal. The dominant triplet pairing is consistent with the experimental upper critical field exceeding the Pauli limit.

PACS numbers: 74.20.-z, 74.20.Mn, 74.20.Rp, 71.27.+a, 64.60.ae

Triplet pairing is a special kind of Cooper pairing, most favorably occurs when there are enhanced ferromagnetic-like spin fluctuations. The reason for the enthusiastic search of triplet pairing is twofold. On one hand, triplet pairing is only found in He-III[1] and possibly in Sr₂RuO₄[2], but is otherwise rare in condensed matters. There are singlet-triplet mixtures in noncentrosymmetric materials but the case with dominant triplet component is also rare.[3] Finding a new material with triplet pairing is therefore a challenge. On the other hand, the interest in the search of triplet superconductors is enhanced in view of the fact that under a suitable condition a triplet superconductor may be topologically non-trivial, supporting Majorana modes on the edge or in a vortex core.[4] The Majorana modes satisfy non-Abelian braiding statistics and thus could be used in topological quantum computing.[4, 5]

Recently, a new layered superconductor Bi₄O₄S₃ with $T_c \sim 4.5$ K was discovered.[6] The conduction plane is BiS₂ layer, with weak inter-layer coupling. The layered structure is similar to that in cuprates [7] and iron-based superconductors.[8] Subsequently a family of superconductors containing the same conduction layer were discovered. These include LnO_{1-x}F_xBiS₂ (Ln = La, Nd, Ce, Pr, Yb), [9–13], Sr_{1-x}La_xFBiS₂[14], and La_{1-x}M_xOBiS₂ (M = Ti, Zr, Hf, Th)[15]. In such systems the parent compound is a band insulator or semiconductor. Superconductivity is realized by electron doping, except in Sr_{1-x}La_xFBiS₂. The basic band structure obtained by first principle calculations[16–18] reveals very interesting features. The Fermi surface is two-dimensional like and has a good extent of nesting. As a function of doping, the Fermi surface evolves from X-Y pockets encircling the midpoints on the edges of the Brillouine zone (BZ) to the Γ -M pockets encircling the center and the corner of the BZ via a Lifshitz transition. Around this point, the density of states is higher and would make the system susceptible to various forms of instabilities upon the electron-electron interactions. Moreover, there are significant spin-orbital couplings (SOC) due to the

heavy Bismuth atoms.

At present there is no consensus on the cause of Cooper pairing in these materials. Opinions range from Cooper pairing caused by soft phonon modes[17, 18] to pairing caused by strong correlation[19, 20]. As single crystal samples are not available at the present stage, experimental evidences that would distinguish one versus the other mechanism are rare. One exception is the experimental upper critical field (for grain samples) which seems to exceed the Pauli limit, suggesting triplet pairing.[21] The other exception is the large ratio $2\Delta/T_c \sim 17$ observed recently,[21] implying that the underlying pairing mechanism is likely unconventional. We are thus motivated to investigate the effect of electron correlations. We use the singular mode functional renormalization group (SMFRG) method, which has been successful in many contexts even when the strength of the electron-electron interaction is intermediate.[23–27] The advantage of FRG [28] is the capability of surveying all electronic instabilities at the same time.[23–27, 29] The SMFRG developed for fully antisymmetrized interactions has been recently utilized in the search of correlation driven topological superconductors,[24] and will be applied here given the SOC.

The main results in this Letter are as follows. We find the pairing in BiS₂-based superconductors has a dominant triplet component, apart from a subdominant singlet component due to SOC. The pairing respects time-reversal symmetry, and the gap changes sign on spin-split Fermi pockets. With respect to joint spin-lattice operations (denoted by a superscript * henceforth), the pairing gap has $d_{x^2-y^2}^*$ -wave symmetry, and changes from being nodeless to nodal as the Fermi surface evolves from X-Y pockets to Γ -M pockets around the Lifshitz points. The nodeless $d_{x^2-y^2}^*$ -wave phase can be categorized as a time-reversal-invariant weak topological superconducting phase. The dominant triplet pairing is consistent with the experimental upper critical field exceeding the Pauli limit.

We start by describing the model. Since the inter-

layer coupling is weak we consider a one-layer model for brevity, although a unit cell contains two layers. (We shall come to the effect of inter-layer coupling before closing.) The conduction bands are mainly derived from the bismuth p_x and p_y orbitals. We write the non-interacting part of the hamiltonian as, $H_0 = \sum_{\mathbf{k}} \psi_{\mathbf{k}}^\dagger (\chi_{\mathbf{k}} + \xi_{\mathbf{k}}) \psi_{\mathbf{k}}$ where $\psi = (C_{x\uparrow}, C_{y\uparrow}, C_{x\downarrow}, C_{y\downarrow})^T$ is a four-spinor, with $C_{x/y}$ annihilating the bismuth $p_{x/y}$ orbital. The spin-independent part $\chi_{\mathbf{k}}$ can be obtained from Ref.[6], where we observe that the leading second-neighbor hoppings dominates the first-neighbor ones. This feature turns out to have profound consequences in the pairing function (see below). The SOC part can be written as, up to the first neighbors, $\xi_{\mathbf{k}} = -\lambda\tau_2\sigma_z - \gamma_s(\sin k_x\sigma_y - \sin k_y\sigma_x) - \gamma_d(\sin k_x\sigma_y + \sin k_y\sigma_x)\tau_3$. Here τ and σ are Pauli matrices acting on orbital and spin bases. The λ -term is the atomic SOC and the γ -terms are simplest symmetry-allowed Rashba-type couplings (in the absence of mirror symmetry about z). A fit to a relativistic band structure calculation [17] suggests $(\lambda, \gamma_s, \gamma_d) \sim (0.5, 0.02, 0.16)\text{eV}$. (There is some uncertainty in $\gamma_{s,d}$, but it is not crucial in the later development since we get closely similar results by decimating or doubling $\gamma_{s,d}$.) The band structure is shown in Fig.1(a), where we have four spin-split bands, and the horizontal lines denote the Fermi levels to be considered later. The normal state density of states is shown in Fig.1(b), which is enhanced around the Lifshitz points indicated by the arrows.

The interacting part of the hamiltonian we consider is, written in real space, $H_I = U \sum_{i,a} n_{ia\uparrow} n_{ia\downarrow} + U' \sum_{i,a>b} n_{ia} n_{ib} + J \sum_{i,a>b,\sigma,\sigma'} \psi_{ia\sigma}^\dagger \psi_{ib\sigma} \psi_{ib\sigma'}^\dagger \psi_{ia\sigma'} + J' \sum_{i,a,b} \psi_{ia\uparrow}^\dagger \psi_{ia\downarrow}^\dagger \psi_{ib\downarrow} \psi_{ib\uparrow} + V \sum_{\langle ij \rangle} n_i n_j$. Here a and b label the orbitals, (U, U', J, J') are local interactions, and V is the Coulomb interaction between nearest neighbors. We use the standard relation $U = U' + 2J$ and $J = J'$ to reduce the number of independent parameters. In the metallic state we expect $V \ll U$, and for the p -orbital system we expect $J \ll U$. For simplicity we set $J = V = U/6$, as fine tuning around this setting leads to closely similar results. We have to estimate U . Consider partial screening from particle-hole excitations out of the energy window W of the band structure under concern.[30] The dielectric constant in this picture is roughly $\varepsilon \sim 1 + aV_c/W$, where a is a number of order unity, and V_c is the local unscreened Coulomb interaction for the p -orbitals. Assuming $W = 5 \sim 6\text{eV}$, $a = 0.5 \sim 1$ and $V_c = 20 \sim 30\text{eV}$, we find V_c/ε ranges from 3eV to 8eV . In the absence of a better estimate, we simply take $U \in [2, 10]\text{eV}$. We stress that the Mott physics is not relevant here for two reasons. First the relevant electron filling is far from half filling per atom per orbital. Second, the p -orbitals are fully hybridized so that the interaction projected on the band basis is reduced by roughly a factor of two. This reasoning justifies the use of FRG below.

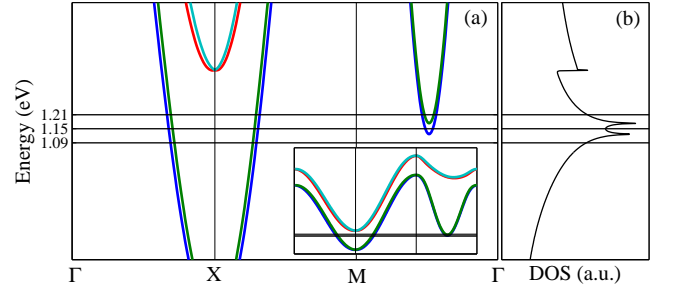


FIG. 1: (Color online) (a) Spin-split band structure along high symmetry cuts. The inset is a global view. (b) Normal state density of states. The three horizontal lines indicate three typical cases to be studied in details. The cusp-like peaks follow from the enhanced density of states at the Lifshitz points.

An interacting system would exhibit collective fluctuations in particle-particle (pp) and particle-hole (ph) channels, the exact nature of which depends on the energy scale when they are observed. In our SMFRG scheme, the fully antisymmetrized effective interaction vertex at a given scale is decoupled as,

$$V^{\alpha\beta;\gamma\delta}(\mathbf{k}, \mathbf{k}', \mathbf{q}) \rightarrow \sum_m S_m(\mathbf{q}) \phi_m^{\alpha\beta}(\mathbf{k}, \mathbf{q}) [\phi_m^{\gamma\delta}(\mathbf{k}', \mathbf{q})]^*, \quad (1)$$

either in the pp or ph channels. Here $\alpha, \beta, \gamma, \delta$ are (spin, orbital) labels, \mathbf{q} is the collective wavevector, and \mathbf{k} (or \mathbf{k}') the internal momentum of the Fermion bilinears $\psi_{\mathbf{k}+\mathbf{q},\alpha}^\dagger \psi_{-\mathbf{k},\beta}^\dagger$ and $\psi_{\mathbf{k}+\mathbf{q},\alpha}^\dagger \psi_{\mathbf{k},\beta}$ in the pp and ph channels, respectively. The SMFRG provides coupled flow of all channels versus a decreasing energy scale Λ (the infrared limit of the Matsubara frequency in our case). In the following we define, in a specific channel, $S(\mathbf{q})$ as the leading eigenvalue for a given \mathbf{q} , and S the globally leading one for all \mathbf{q} . The most attractive and fast growing eigenvalue represents the dominant ordering tendency with an associated collective momentum \mathbf{Q} and eigenfunction (or form factor) $\phi(\mathbf{k}, \mathbf{Q})$, in the respective channel.[31] The technical details can be found elsewhere.[24]

First we consider an electron filling $n = 0.45$ (per site), a filling level below the Lifshitz points. The Fermi level corresponds to the lowest horizontal line in Fig.1. The spin-split Fermi surfaces are shown in Fig.2(a) and (b), with electron pockets around X and Y points of the BZ. For $U = 8\text{eV}$ and $J = V = U/6$, the FRG flow is shown in Fig.2(c). The interaction S_{ph} is initially screened slightly, re-enhanced in the intermediate stage and levels off at low energy scales because of lack of phase space for low energy p-h excitations. The associated momentum evolves (as indicated by the arrows) but eventually settles down on $\mathbf{Q} \sim (\pi, \pi)$. Inspection of the form factor ϕ_{ph} shows that it describes predominantly site-local spin fluctuations. However, from $S_{\text{ph}}(\mathbf{q})$ (obtained at the final stage of the RG flow) shown in the inset, we see a comparable peak at $\mathbf{q} = 0$, and we find it is also spin-like. Attractive

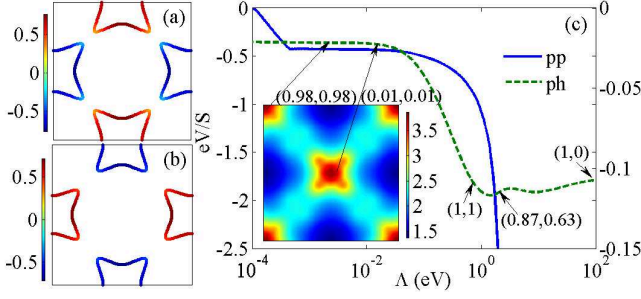


FIG. 2: (Color online) Results for $n = 0.45$. Here (a) and (b) shows the spin-split Fermi surfaces. The color scale denotes the pairing gap thereon. (c) FRG flow of $1/S_{pp,ph}$ versus Λ associated with the left/right scale. Arrows indicate snapshots of the leading \mathbf{q}/π for S_{ph} during the flow. The inset shows $\ln|S_{ph}(\mathbf{q})|$ in the momentum space at the final energy sale.

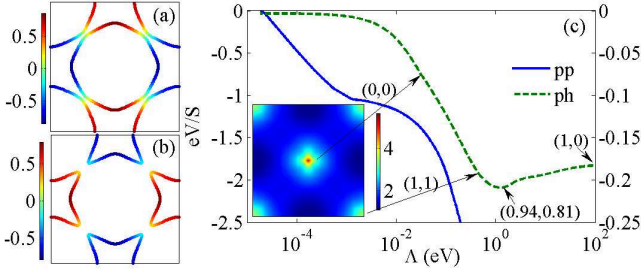


FIG. 3: (Color online) The same plot as Fig.2 except that $n = 0.55$ and $U = 4.5\text{eV}$.

pairing interaction S_{pp} is induced as S_{ph} is enhanced via the mutual overlap between the channels. There is a cusp in the evolution of S_{pp} , which is in fact a level crossing of the leading pairing function $\phi_{pp}(\mathbf{k})$. Eventually S_{pp} diverges, implying a superconducting phase. Henceforth we write the matrix pairing function in the orbital basis as $\phi_{pp}(\mathbf{k}) = (g_{\mathbf{k}} + \gamma_{\mathbf{k}})i\sigma_y$, with singlet and triplet parts $g_{\mathbf{k}}$ and $\gamma_{\mathbf{k}}$, respectively. These components can be expressed in terms of lattice harmonics $c_{x/y} = \cos k_{x/y}$ and $s_{x/y} = \sin k_{x/y}$ as well as the Pauli matrices τ and σ . In the present case, we find $g_{\mathbf{k}} \sim -(0.03 + 0.02c_x c_y)\tau_3$ and $\gamma_{\mathbf{k}} \sim -0.02(\sigma_x s_y + \sigma_y s_x) + 0.15(\sigma_x s_y c_x + \sigma_y s_x c_y) - 0.63\tau_1(\sigma_x s_x c_y + \sigma_y s_y c_x) + 0.27\tau_3(\sigma_x s_y c_x - \sigma_y s_x c_y)$. There are some remarkable features here. First, the singlet part $g_{\mathbf{k}}$ transforms as d -wave (via τ_3), but the amplitude is relatively small. The dominant part is the $\tau_{1,3}$ -terms in $\gamma_{\mathbf{k}}$ describing triplet pairing on second-neighbor bonds. The reason can be traced back to the dominant second-neighbor hoppings in $\chi_{\mathbf{k}}$ mentioned previously. The triplet component is consistent with the existence of small- \mathbf{q} features in $S_{ph}(\mathbf{q})$ discussed above. It is in fact also in harmony with the large- \mathbf{q} features of $S_{ph}(\mathbf{q})$ since on second-neighbor bonds such spin correlations are also ferromagnetic-like. The d -wave-like singlet component is also consistent with the large- \mathbf{q} spin

correlations. The singlet and triplet components coexist due to the SOC, and we observe that they transform identically upon *joint spin-lattice operations*. Second, the pairing function respects time-reversal symmetry. This enables us to project ϕ_{pp} on the band basis as $\Delta_{\mathbf{k}} = \langle \mathbf{k} | \phi_{pp}(\mathbf{k}) | -\mathbf{k} \rangle^* = \langle \mathbf{k} | g_{\mathbf{k}} + \gamma_{\mathbf{k}} | \mathbf{k} \rangle$, where $|\mathbf{k}\rangle$ is a Bloch state and $|- \mathbf{k}\rangle = T|\mathbf{k}\rangle$ is the time-reversal of $|\mathbf{k}\rangle$. Thus $\gamma_{\mathbf{k}}$ would lead to sign changes of $\Delta_{\mathbf{k}}$ on spin-split bands in the same way as a Rashba-term splits the bands. The subdominant singlet component $g_{\mathbf{k}}$ does not alter this conclusion. These observations are exactly reflected in Fig.2(a) and (b) where $\Delta_{\mathbf{k}}$ is shown by the color scale. The d -wave like sign structure is what we anticipated from inspection of the pairing function in the orbital basis. We dub this kind of pairing symmetry as $d_{x^2-y^2}^*$ -wave with the star emphasizing joint spin-lattice operations. We observe that $\Delta_{\mathbf{k}}$ is nodeless, and the sign changes twice from pockets to pockets (encircling T-invariant momenta). This is in fact classified as a T-invariant weak topological superconducting phase.[32] There are gapless edge states in this phase, although they are not topologically protected because of the weak topology. Thus BiS₂ may be a good candidate to explore T-invariant topological superconductivity.

We now tune the fermi level to lie in between the Lifshitz points, as indicated by the middle horizontal line in Fig.1. The filling level here is $n = 0.55$ per site. The spin-split Fermi surface shown in Fig.3 form two hole-like Γ -M pockets (a) and two electron-like X-Y pockets (b). At this filling the density of states is higher, so we use $U = 4.5\text{eV}$ and $J = V = U/6$. ($U > 5$ leads to ferromagnetic instability otherwise). The FRG flow is shown in Fig.3(c). In the ph-channel the momentum settles down at $\mathbf{Q} \sim 0$ with predominant site-local spin fluctuations. The final $S_{ph}(\mathbf{q})$ in the inset is similar to that in the previous case, except the peak at the zone center is much stronger. The existence of such fluctuations would again favor triplet pairing. Indeed, at the divergence scale of S_{pp} , we check the pairing function $\phi_{pp}(\mathbf{k})$ to find $g_{\mathbf{k}} \sim -0.01\tau_3 - 0.01i\tau_2 s_x s_y$ and $\gamma_{\mathbf{k}} \sim 0.11(\sigma_x s_y c_x + \sigma_y s_x c_y) - 0.58\tau_1(\sigma_x s_x c_y + \sigma_y s_y c_x) + 0.39\tau_3(\sigma_x s_y c_x - \sigma_y s_x c_y)$. The triplet pairing on second neighbor bonds again dominates. Furthermore, the gap projected on the Fermi pockets in (a) and (b) shows that it is again a $d_{x^2-y^2}^*$ -wave pairing. However, the gap is now nodal in (a) since the Γ -M pockets are cut by the nodal direction of a $d_{x^2-y^2}$ function. Instead, the gap in (b) remains nodeless on the X-Y pockets which avoid the nodal line.

To have better systematics, we further tune the fermi level to lie above the Lifshitz points, as shown by the upper horizontal line in Fig.1. The filling level is $n = 0.64$ here. The spin-split Fermi surface in Fig.4(a) and (b) consists of two pairs of Γ -M pockets. For $U = 6\text{eV}$ and $J = V = U/6$, the FRG flow is shown in Fig.4(c). At the final stage, S_{ph} is associated with a small incom-

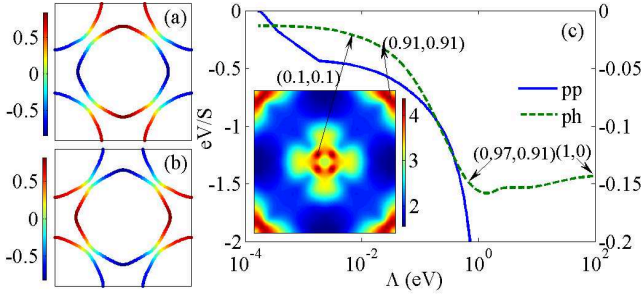


FIG. 4: (Color online) The same plot as Fig.2 except that $n = 0.64$ and $U = 6\text{eV}$.

mensurate momentum $\mathbf{Q} \sim (0.1, 0.1)\pi$, and we check that it describes predominantly spin fluctuations. The final $S_{\text{ph}}(\mathbf{q})$ in the inset shows that there are also slightly weaker peaks near the zone corners. The pairing interaction diverges via a final level crossing. The components of the pairing function can be written as, $g_{\mathbf{k}} \sim -(0.02 + 0.06c_x c_y)\tau_3$ and $\gamma_{\mathbf{k}} \sim -0.01(\sigma_x s_y + \sigma_y s_x) + 0.11(\sigma_x s_y c_x + \sigma_y s_x c_y) - 0.60\tau_1(\sigma_x s_x c_y + \sigma_y s_y c_x) + 0.36\tau_3(\sigma_x s_y c_x - \sigma_y s_x c_y)$. Similar to the previous cases, the triplet component dominates, and the pairing function has $d_{x^2-y^2}^*$ -wave symmetry. This is more clearly seen in Fig.4(a) and (b) for the gap projected on the Fermi surfaces. We notice that because of the comparable large- \mathbf{q} spin fluctuations, the second leading pairing function has s_{\pm}^* -wave symmetry, with sign changes from Γ - to M -pockets but still with dominant triplet component.

We have performed systematic calculations for other values of bare interaction parameters and other filling levels. The results are summarized as a schematic phase diagram in Fig.5. The same type of pairing functions are obtained at lower values of U , but with a rapidly decreasing divergence scale. Around the Lifshitz points, the system develops ferromagnetism (antiferromagnetism) for $U = 5 \sim 7.5\text{eV}$ ($U > 7.5\text{eV}$). Antiferromagnetism also appears at doping levels away from the Lifshitz points, but only at still larger values of U . That the antiferromagnetic state is favored at large U is reflected in the cases examined above: spin fluctuations at large wavevectors are always more efficiently enhanced in the early stage of RG flow. For lower values of U , there is a large parameter space favoring the triplet-dominant pairing as discussed above.

Finally we discuss how the results survive in a two-layer model. There will be an inter-layer hopping along the bonds $(\pm 0.5a, \pm 0.5a, \pm b)$ where a (or b) is the in-plane lattice constant (or interlayer distance), with hopping integral t_{\perp} . On the other hand, the Rashba-term reverses sign on the two layers by symmetry. We included these two ingredients and performed SMFRG to find that there are no essential difference in the results. The inter-plane pairing is negligible for a reasonably small t_{\perp} , so we only have to compare the in-plane pairings. We find the

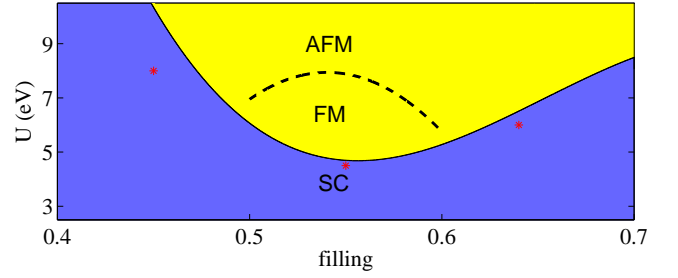


FIG. 5: (Color online) A schematic phase diagram versus U and electron filling, assuming $J = V = U/6$. The stars show the cases discussed in the text. Fine tuning around $J = V = U/6$ does not lead to qualitative changes.

only effect in the double-layer model is that the singlet component $g_{\mathbf{k}}$ changes sign from one to the other layer.

To conclude, we find that the newly discovered BiS_2 -based superconductors may have a dominant triplet component. The pairing respects time-reversal symmetry, and the gap changes sign on spin-split Fermi pockets. In view of combined spin-lattice rotations, the gap function has a $d_{x^2-y^2}^*$ -wave symmetry. It changes from being nodeless to nodal as the Fermi surface evolves from X-Y pockets to Γ -M pockets around the Lifshitz points. The nodeless $d_{x^2-y^2}^*$ -phase is a time-reversal-invariant weak topological superconductor. The dominant triplet pairing is consistent with the experimental upper critical field exceeding the Pauli limit.

QHW thanks Fa Wang, Dung-Hai Lee and Xian-Gang Wan for helpful discussions. The project was supported by NSFC (under grant No.10974086 and No.11023002) and the Ministry of Science and Technology of China (under grant No.2011CBA00108 and 2011CB922101).

-
- [1] For a review see D. Vollhardt, and P. Wölfle, *The Superfluid Phases of Helium* (Taylor and Francis, USA 1990).
 - [2] For a review and references see A. P Mackenzie, and Y. Maeno, Rev. Mod. Phys. **75**, 657 (2003).
 - [3] M. Sato, S. Fujimoto, Phys. Rev. B **79**, 094504 (2009); M. Sato, Y. Takahashi, and S. Fujimoto, Phys. Rev. B **82**, 134521 (2010).
 - [4] D. A. Ivanov, Phys. Rev. Lett. **86**, 268 (2001); N. Read and D. Green, Phys. Rev. B **61**, 10267 (2000).
 - [5] C. Nayak, *et al*, Rev. Mod. Phys. **80**, 1083 (2008).
 - [6] Y. Mizuguchi, H. Fujihisa, Y. Gotoh, K. Suzuki, H. Usui, K. Kuroki, S. Demura, Y. Takano, H. Izawa, and O. Miura, Phys. Rev. B **86**, 220510 (2012).
 - [7] J.G. Bednorz and K.A. Muller, Z. Phys. B: Cond. Matt. **64**, 189 (1986).
 - [8] Y. Kamihara, T. Watanabe, M. Hirano, and Hideo Hosono, J. Am. Chem. Soc. **130**, 3296 (2008).
 - [9] Y. Mizuguchi, S. Demura, K. Deguchi, Y. Takano, H. Fujihisa, G. Y., H. Izawa, and O. Miura, J. Phys. Soc. Jpn **81**, 114725 (2012); H. Kotegawa, Y. Tomita, H. Tou, H. Izawa, Y. Mizuguchi, O. Miura, S. Demura, K. Deguchi,

- and Y. Takano, J. Phys. Soc. Jpn. **81**, 103702 (2012).
- [10] S. Demura, Y. Mizuguchi, K. Deguchi, H. Okazaki, H. Hara, T. Watanabe, S. J. Denholme, M. Fujioka, T. Ozaki, H. Fujihisa, et al., J. Phys. Soc. Jpn. **82**, 033708 (2013).
 - [11] R. Jha, A. Kumar, S. K. Singh, and V. P. S. Awana, J. Appl. Phys. **113**, 056102 (2013).
 - [12] J. Xing, S. Li, X. Ding, H. Yang, and H.-H. Wen, Phys. Rev. B **86**, 214518 (2012).
 - [13] S. K. Singh, A. Kumar, B. Gahtori, Shruti, G. Sharma, S. Patnaik, and V. P. S. Awana, J. Am. Chem. Soc. **134**, 16504 (2012).
 - [14] X. Lin, X. Ni, B. Chen, X. Xu, X. Yang, J. Dai, Y. Li, X. Yang, Y. Luo, Q. Tao, G. Cao, and Z. Xu, Phys. Rev. B **87**, 020504 (2013).
 - [15] D. Yazici, K. Huang, B. D. White, I. Jeon, V. W. Burnett, A. J. Friedman, I. K. Lum, M. Nallaiyan, S. Spagna, and M. B. Maple, arXiv: 1303.6216.
 - [16] H. Usui, K. Suzuki, and K. Kuroki, Phys. Rev. B **86**, 220501 (2012).
 - [17] X.-G. Wan, H.-C. Ding, S. Y. Savrasov, and C.-G. Duan, Phys. Rev. B **87**, 115124 (2013).
 - [18] T. Yildirim, Phys. Rev. B **87**, 020506 (2013).
 - [19] G. Martins, A. Moreo, and E. Dagotto, Phys. Rev. B **87**, 081102 (2013).
 - [20] Y. Liang, X. Wu, W.-F. Tsai, and J.-P. Hu, arXiv: 1211.5435.
 - [21] S. Li, H. Yang, D.-L. Fang, Z.-Y. Wang, J. Tao, X. Ding, and H.-H. Wen, arXiv: 1304.3354.
 - [22] Gap ratio from STM by Wen's group.
 - [23] W.-S. Wang, Y.-Y. Xiang, Q.-H. Wang, F. Wang, F. Yang, and D.-H. Lee, Phys. Rev. B **85**, 035414 (2012).
 - [24] Y.-Y. Xiang, W.-S. Wang, Q.-H. Wang, and D.-H. Lee, Phys. Rev. B **86**, 024523 (2012).
 - [25] W.-S. Wang, Z.-Z. Li, Y.-Y. Xiang, and Q.-H. Wang, Phys. Rev. B **87**, 115135 (2013).
 - [26] Y.-Y. Xiang, F. Wang, D. Wang, Q.-H. Wang, and D.-H. Lee, Phys. Rev. B **86**, 134508 (2012).
 - [27] Y.-Y. Xiang, Y. Y., W.-S. Wang, Z.-Z. Li, Q.-H. Wang, arXiv: 1305.1806.
 - [28] C. Wetterich, Nucl. Phys. B, **352**, 529 (1991).
 - [29] See, *e.g.*, M. Salmhofer and C. Honerkamp, Prog. Theor. Phys. **105**, 1 (2001); F. Wang, H. Zhai, Y. Ran, A. Vishwanath, and D.-H. Lee, Phys. Rev. Lett. **102**, 047005 (2009).
 - [30] See, *e.g.*, T. Miyake and F. Aryasetiawan, Phys. Rev. B **77**, 236805 (2008); T. O. Wehling, E. Sasiaglu, C. Friedrich, A. I. Lichtenstein, M. I. Katsnelson and S. Blugel, Phys. Rev. Lett. **106**, 236805 (2011).
 - [31] Notice that all **Q**-vectors have symmetry images, and could evolve with the running energy scale.
 - [32] X.-L. Qi and S.-C. Zhang, Rev. Mod. Phys. **83**, 1057 (2011).